Thermodynamics of Ammonia and Ammonium Ion at the Aqueous Solution−Air Interfaces

ARTICLE *in* THE JOURNAL OF PHYSICAL CHEMISTRY C · JUNE 2014

Impact Factor: 4.77 · DOI: 10.1021/jp312110w

2 AUTHORS:

Cen-Feng Fu
University of Science and Technology of China
4 PUBLICATIONS **26** CITATIONS
SEE PROFILE

Shan Xi Tian
University of Science and Technology of China
88 PUBLICATIONS **662** CITATIONS
SEE PROFILE

THE JOURNAL OF PHYSICAL CHEMISTRY C

Article

pubs.acs.org/JPCC

Thermodynamics of Ammonia and Ammonium Ion at the Aqueous Solution−Air Interfaces

Cen-Feng Fu and Shan Xi Tian*

Hefei National Laboratory for Physical Sciences at the Microscale and Department of Chemical Physics, University of Science and Technology of China, Hefei, Anhui 230026, China

ABSTRACT: Ammonia (NH_3) and ammonium ion (NH_4^+) are two main pollutants of Earth's surface water system. Toward an understanding of the microscopic structures and thermodynamic properties of NH_3 and NH_4^+ (along with halogen anion Cl^-, Br^-, or I^-) at the aqueous solution−air interfaces, all-atom molecular dynamics simulations are performed with different solute concentrations and at various temperatures. The surface propensities of NH_3, Br^-, and I^- species are predicted, while the NH_4^+ is repelled from the interface. The solute concentration strongly influences the spatial distributions of NH_3, Cl^-, Br^-, and I^- near the interface; moreover, the specific temperature effects on the surface charge, molecular orientation, and surface tension are demonstrated.

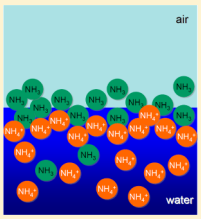

1. INTRODUCTION

Water pollution has become a serious crisis, most directly to aquatic life and human beings. Ammonia (NH_3) and the ammonium ion (NH_4^+) are two main criminals in pollution of the Earth's surface water system.[1] NH_3 and NH_4^+ can be converted into each other, depending on both pH and temperature of the solutions. In the chlorination of drinking water, a small amount of NH_3 and NH_4^+ as well as organics and reducing agents can eliminate the disinfecting ability of chlorine. Basic knowledge about the properties of NH_3/NH_4^+ aqueous solution and interfaces is imperative to further optimize the current drinking water techniques.

A specific ion effect on the solution−air interface was recently reviewed.[2,3] Theoretical simulations of the single ion in an aqueous slab were performed using nonpolarizable force fields.[4−6] Nevertheless, no propensity of the ions at the solution−air interface was observed if polarization interactions in the interface were neglected by using the nonpolarizable force fields.[2] The solution−air interface as a specific environment is different from the bulk solution, and in the former the polarization interaction usually plays an essential role.[2,3,7−9] Dang et al.[10,11] investigated the mechanism of ion binding to the liquid−vapor interface by performing the potential of mean force simulations with nonpolarizable and polarizable force fields. For the halogen anions (Br^- and I^-), they found a free energy minimum near the Gibbs surface under the polarizable model, while a monotone increased free energy profile by using the nonpolarizable model.[10,11] Employing the polarizable force field, this landscape of free energy profile was further proved by other molecular dynamics (MD) simulations for the sodium-halide aqueous solution−air interface.[7,12−16] The halogen anions distinctly exhibit the surface propensity in a decreasing order of $I^- > Br^- > Cl^-$, while the sodium cation prefers the interior solvation. The concentration enhancement further reduced the surface propensities of the heavier halogen anions but induced the sodium cations to form a subsurface peak near the surface,[15] thus an electrical double layer near the surface was formed.[17] However, the above prediction about the surface propensity for the heavier halogen ions is contrary to the standard theory of the surfaces of electrolytes.[18] Subsequently, to obtain a more complete description of specific ion effects, the NO_3^-, N_3^-, SO_4^{2-}, H_3O^+, and OH^- ions at the solution−air interface were also investigated by MD simulations.[19−24] The NO_3^-, N_3^-, and H_3O^+ ions were found around the solution−air interface, while most of the SO_4^{2-} and OH^- were far away from the interface. Moreover, Yang et al.[25] found that the surface propensity of the anions was more visible than that of the cations. In combination with MD simulation, the surface structure of sulfuric acid solution was revealed by the sum frequency generation (SFG) measurements.[26,27] Recently, the adsorption processes of ions into liquid−vapor interfaces of water−methanol mixtures[28] and the liquid−liquid interface of water−decane[29] were also investigated.

A few experimental and theoretical studies have focused on the properties of ammonia and the ammonium ion at the aqueous solution−air interface.[30−37] Using the SFG spectroscopy, the structural properties of the solution−air interfaces of the ammonia[30,31] and NH_4^+ solution[34,37] were reported. The free energy transfer, the orientational preference, and the hydrogen-bonded structure and dynamics of the NH_3 molecules at the solution−air interface were studied with the MD simulations.[32,33,35,36] Nevertheless, no systematic studies on the liquid−vapor interfaces of NH_3 and NH_4^+ solutions were carried out; in particular, their thermodynamic differences were still unknown. In the present work, the microscopic structures and thermodynamic properties of NH_3 and NH_4^+ at the interface are investigated by using all-atom MD simulations. NH_3 and $NH_4^+X^-$ (X^- = Cl^-, Br^-, and I^-) are soluble in water, and the latter compounds are dissolved into a halogen anion X^- and the weak base cation NH_4^+. Both NH_3 and NH_4^+ are the hydrogen-bond donors; meanwhile, NH_3 can also act as the hydrogen-bond acceptor in aqueous solution. Therefore, these

Received: December 9, 2012
Revised: June 2, 2013
Published: June 4, 2013

Table 1. Force Field Parameters Used in This Work[a]

		q (au)	μ_x (au)	μ_z (au)	Q_{xx} (au)	Q_{yy} (au)	Q_{xz} (au)	Q_{zz} (au)	α (Å^3)	R^0 (Å)	ε (kcal mol^{-1})
Cl^-	Cl	−1.00000	0.00000	0.00000	0.00000	0.00000	0.00000	0.00000	4.0000	4.1300	0.3400
Br^-	Br	−1.00000	0.00000	0.00000	0.00000	0.00000	0.00000	0.00000	5.6500	4.3800	0.4300
I^-	I	−1.00000	0.00000	0.00000	0.00000	0.00000	0.00000	0.00000	7.2500	4.6600	0.5200
NH_3	N	−0.57960	0.15842	0.06469	−0.43288	0.27280	−0.28801	0.16008	1.0730	3.7100	0.1050
	H	0.19320	−0.03286	−0.08851	−0.04741	0.04478	0.01653	0.00263	0.4960	2.7000	0.0200
NH_4^+	N	−0.22892	0.00000	0.00000	0.00000	0.00000	0.00000	0.00000	1.0730	3.7100	0.1050
	H	0.30723	0.00000	0.04225	−0.07085	−0.07085	0.00000	0.14170	0.4960	2.4800	0.0115
H_2O	O	−0.51966	0.00000	0.14279	0.37928	−0.41809	0.00000	0.03881	0.8370	3.4050	0.1100
	H	0.25983	−0.03859	−0.05818	−0.03673	−0.10739	−0.00203	0.14412	0.4960	2.6550	0.0135

[a] q is the atomic charge; μ_i are the atomic dipole; Q_{ij} are the atomic multipoles (chloride atoms and anions: Q_{ij} = 0 au); α is the polarizability; R^0 is the minimum energy distance; and ε is the potential well depth.

two species should play distinctly different roles in destruction of the hydrogen-bond net of liquid water. What is more, the influences of solute concentration (c) and temperature (T) on the molecular structure and thermal property of the interface will be investigated.

2. COMPUTATIONAL METHODS

AMOEBA developed by Ponder and co-workers[38−40] is a typical polarizable force field which treats electrostatic interactions by using polarizable atomic multipoles. The structural properties of small clusters, liquid water, and ice predicted by using this force field were in excellent agreement with experimental and high-level quantum mechanical results;[39] moreover, the experimental data about the thermodynamics properties of some electrolytic solutions were accurately reproduced.[41] This force field was examined comprehensively by the structural minimizations of the clusters containing a single halogen anion and 1−6 water molecules and by MD simulations for the Na^+X^- (X = Cl^-, Br^-, and I^-) solution−air interface.[16] The solvation shell structures in the clusters and the propensity increasing order of $Cl^- < Br^- < I^-$ for the Na^+X^- (X = Cl^-, Br^-, and I^-) solution−air were successfully predicted,[16] in accord with the results of the quantum chemistry calculations and the MD simulations by using the other polarizable force fields.[2,7,14,24] Due to the possible polarizations of NH_3, NH_4^+, and halogen anions at the interface, the polarizable force field AMOEBA 09[38−40] was used in the present MD simulations for the inhomogeneous solution−air systems. The parameters of the AMOEBA 09 force field[38−40] used here were listed in Table 1.

All MD simulations were performed with the TINKER[42] modeling package. Four solutes, NH_3, $NH_4^+Cl^-$, $NH_4^+Br^-$, and $NH_4^+I^-$, were considered, and the pure water−air interface was also simulated for comparison. The interface systems with three different solute concentrations, c = 0.55, 1.07, and 2.05 M, were simulated at T = 300 K. Additionally, the simulations at the other three temperatures, 280, 320, and 340 K, were performed for these four interface systems with the solute concentration c = 1.07 M. Each interface was mimicked with a slab containing 500 water molecules and an additional 5, 10, or 20 solute molecules for the different concentrations c = 0.55, 1.07, or 2.05 M, respectively. Those molecules were put into a 25.0 Å (x) × 25.0 Å (y) × 75.0 Å (z) rectangular box which was implemented with the periodic boundary condition in three dimensions. Initially, the solute molecules were scattered randomly in the box; then the system structures were optimized to a root mean square (rms) gradient per atom of 0.1 kcal mol^{-1} Å^{-1} with induced dipoles converged to 0.01 D rms. Subsequently, a 5.0−10.0 ns MD simulation in the constant volume and temperature (NVT) ensemble was performed to equalize the system. Finally, another 5.0 ns MD simulation in the NVT ensemble was carried out for the product-collecting simulation. In all MD simulations, the velocity Verlet algorithm[43] with a 1.0 fs step was used to integrate Newton's equations of motion. The Berendsen weak-coupling thermostat[44] with a coupling time of 0.1 ps was employed to regulate the temperature. The cutoff distance for all nonbonded interactions was 9.0 Å. The particle-mesh Ewald method[45] was employed to treat Coulomb interactions. The induced dipoles were converged to 0.01 D rms. All chemical bonds including the hydrogen atom were constrained using the RATTLE algorithm.[46]

3. RESULTS AND DISCUSSION

3.1. Spatial Distribution. To clarify the surface propensities of different ions, we plotted the normalized density (ρ/ρ_b) profiles for the aqueous interfaces of NH_3 and $NH_4^+X^-$ (X^- = Cl^-, Br^-, and I^-) in Figures 1−3. As shown in Figure 1, although NH_3 molecules can melt into liquid water, most of them congregate near the solution−air interface, which accords with the prediction based on the free energy profiles.[35] With

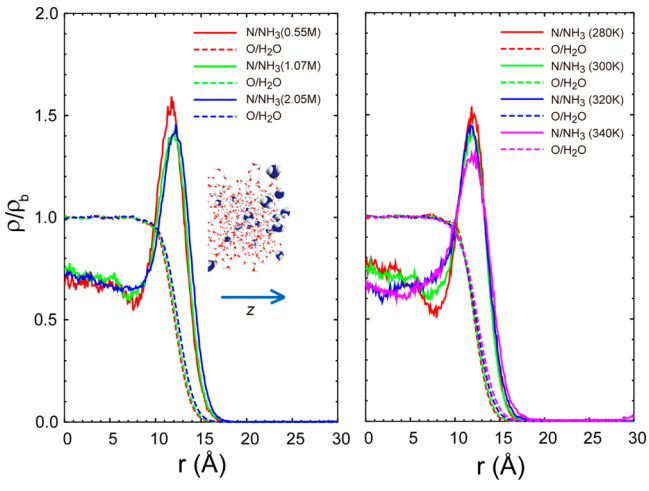

Figure 1. Number densities, ρ, of water oxygen atoms and ammonia nitrogen atoms normalized by the bulk water density, ρ_b, in terms of the distance from the center of the slabs and along the z-direction normal to the interface: (a) for the different ammonia/water concentrations at T = 300 K, the inserted panel shows a snapshot of the equilibrium structures for c = 2.05 M; (b) at the different temperatures for c = 1.07 M.

dx.doi.org/10.1021/jp312110w | J. Phys. Chem. C 2013, 117, 13011−13020

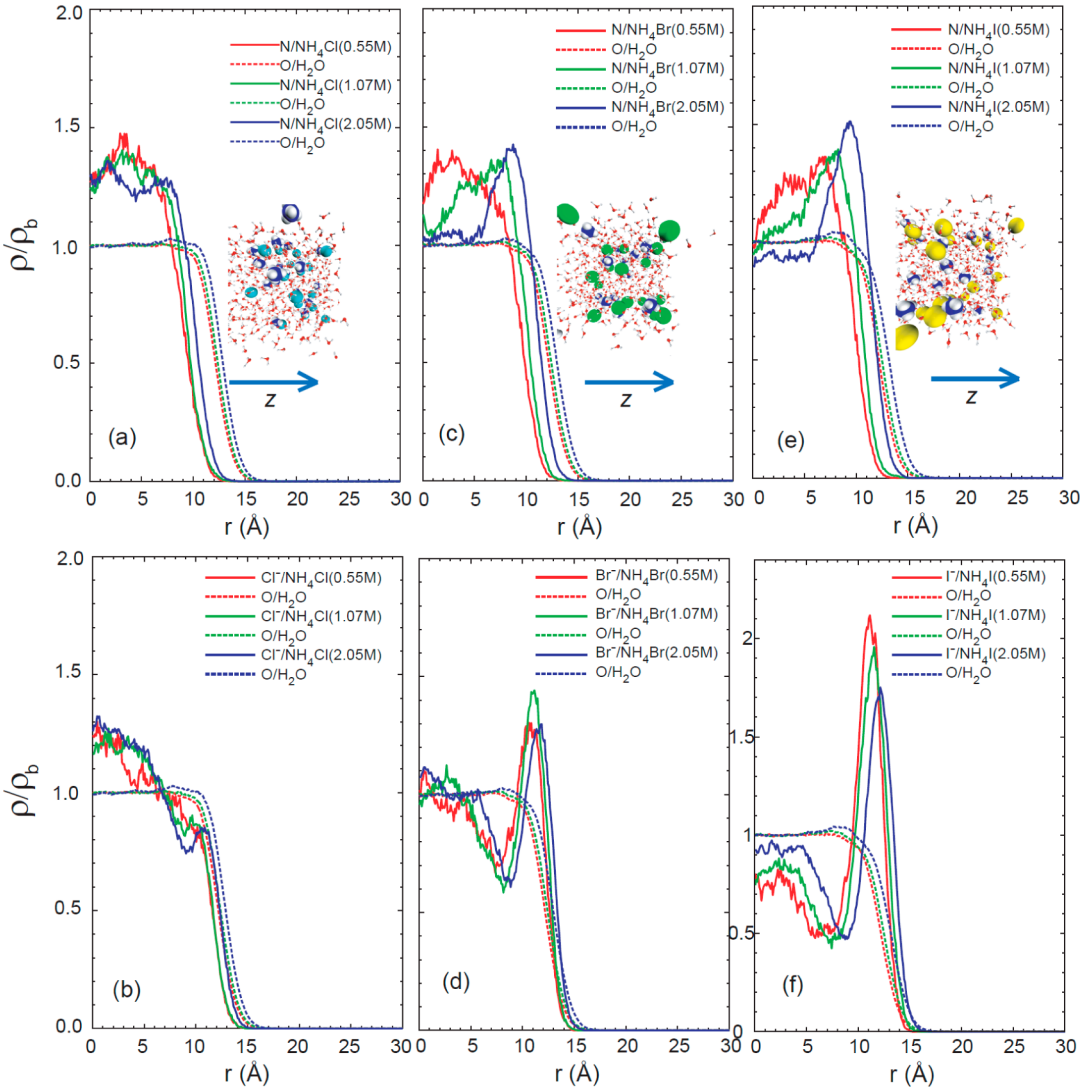

Figure 2. ρ/ρ_b (see definition in caption of Figure 1) with the different $NH_4^+X^-$/water concentrations at T = 300 K: (a), (c), and (e) for NH_4^+(N atom); (b), (d), and (f) for Cl^-, Br^-, and I^-. The insets show the snapshots of the equilibrium structures for c = 2.05 M, Cl^- in cyan, Br^- in green, I^- in yellow.

the c increase from 0.55 to 1.07 M (see Figure 1a), the relative distribution of NH_3 at the interface significantly decreases, which is similar to the observations for the other ions (see Figure 2 and ref 15). Figure 1b shows the remarkable temperature effect on the microstructures. The surface propensity of the NH_3 molecule shows decadence with the temperature increase. At the low temperature T = 280 K, two different NH_3 accumulation areas are found, i.e., the inner region ($0 \sim \pm 7$ Å) and the surface district, while this layer separation is obscured at the higher temperature (e.g., T = 340 K).

The spatial distribution variances with the c values of $NH_4^+X^-$ (X^- = Cl^-, Br^-, I^-) are depicted in Figure 2. When $NH_4^+X^-$ (X^- = Cl^-, Br^-, I^-) dissolves into water, the surface propensities of Br^- and I^- are obvious, while the Cl^- species exhibits little interior preference. This is in line with the surface propensity order of $I^- > Br^- > Cl^-$ predicted for the sodium-halide salt solutions.[14,16] With the increase of c, the surface propensities of both the cation NH_4^+ and anion X^- become more remarkable. However, the clear reduction of the surface intensity of I^- for the higher c value is found in Figure 2f, which is consistent with the tendency of the surface propensity for the SCN^- anion.[15] This mainly arises from the crowding (due to the larger ion size of I^- or SCN^-) and mutual Columbic repulsion of these anions in the interface region, in particular, for the higher concentration.[10,15] On the other hand, for the lower concentration and the smaller ion (see Figure 2d), the intensity peak at ca. 11 Å for the Br^- ion shows an enhancement from 0.55 to 1.07 M of the concentration.

As for the NH_4^+ cation (see Figures 2a, 2c, and 2e), the surface structures are distinctly different from that of NH_3. For the lower c, most of the NH_4^+ cations sink into the solution. However, as shown in Figures 2c and 2e, more and more NH_4^+ cations tend to approach but still be under the surface when the concentration is higher. The surface distribution enhancement of the halogen anions may directly lead to the NH_4^+ congregation underneath the sublayer of anions, which is generally similar to the scenario of the sodium-halide salts, i.e., the nonmonotonic surface distribution of both anions and cations.[14−16] With the increase of c, the electrostatic attraction between the anion and cation is strengthened. Thus, the cations are attracted to the surface due to the significant surface

dx.doi.org/10.1021/jp312110w | J. Phys. Chem. C 2013, 117, 13011−13020

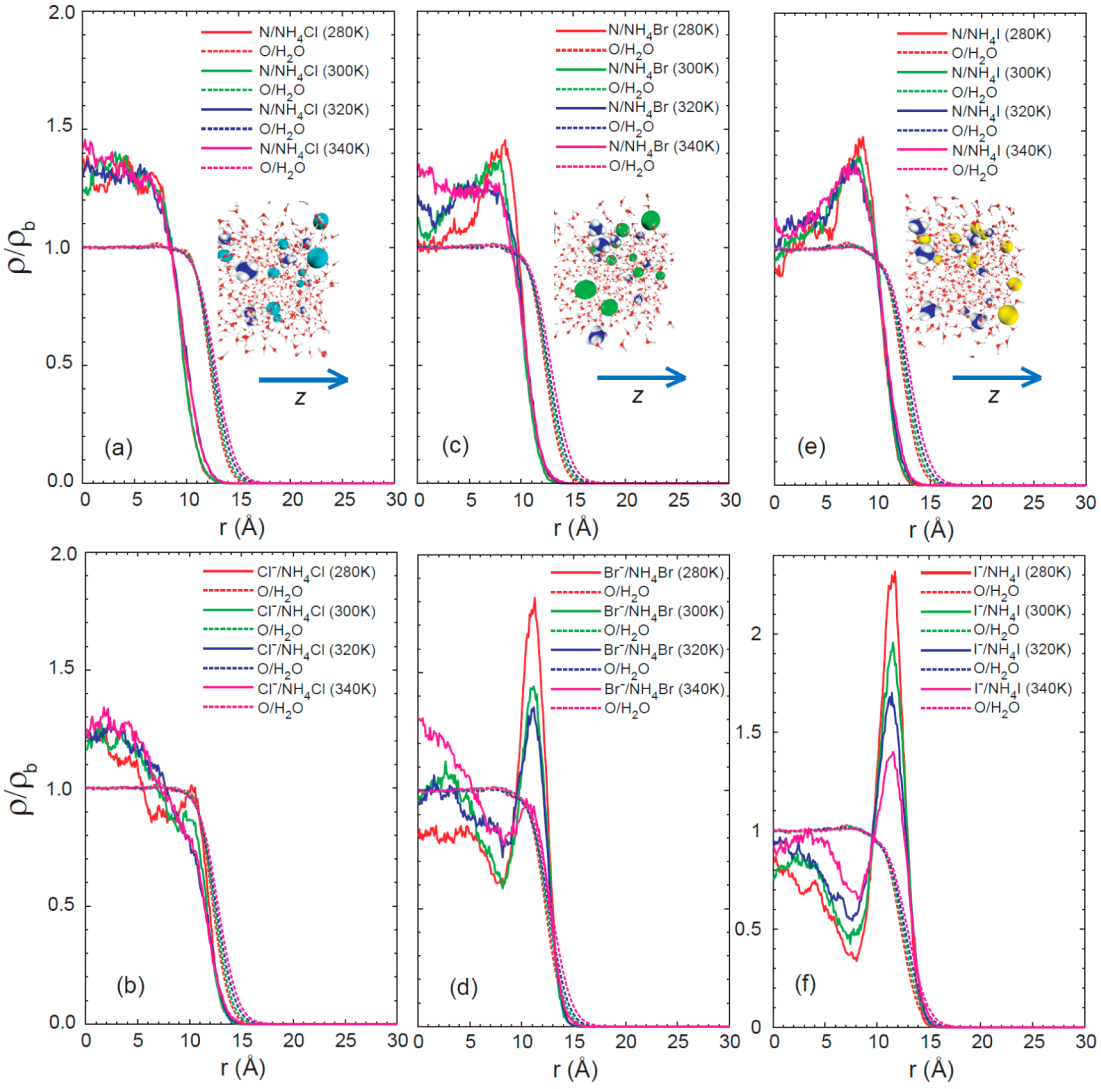

Figure 3. ρ/ρ_b (see definition in caption of Figure 1) at the different temperatures with the $NH_4^+X^-$/water concentrations at c = 1.07 M: (a), (c), and (e) for the NH_4^+(N atom); (b), (d), and (f) for Cl^-, Br^-, and I^-. The insets show the snapshots of the equilibrium structures at T = 280 K, Cl^- in cyan, Br^- in green, I^- in yellow.

propensities of halogen anions; consequently, a subsurface congregation of the cation is formed. Unfortunately, such a simple mechanism of anion−cation attractive interaction is not applicable in elucidating the peculiar structures of the $NH_4^+Cl^-$ interface. In Figures 2a and 2b, when c = 0.55 and 1.07 M, the NH_4^+ are almost repelled from the surface; however, when c = 2.05 M, there is a double layer-like distribution for NH_4^+ (two diffuse peaks at 2 and 8 Å), and the surface peak and sublayer dip for Cl^- are at 11 and 9 Å, respectively. We hypothesize that the layer structure of the Cl^- ions results in an ordered water structure near the surface, and the interactions between NH_4^+ and these ordered water molecules, such as the hydrogen-bonding and the long-range dipole(water)-induced−dipole-(NH_4^+) interactions, further lead to the inhomogeneous distributions of NH_4^+ (shown with a blue line in Figure 2a).

The temperature dependence of the interface structure is the fundamental key toward an understanding of thermal properties of electrolytic solution. In Figure 3, the ρ/ρ_b profiles show the relative distributions of NH_4^+ and the halogen anions at different temperatures T = 280, 300, 320, and 340 K with the common c = 1.07 M. For the halogen anions (see Figures 3b, 3d, and 3f), the surface congregations at the lower temperature T = 280 K are most significant but decline sharply with the rise of temperature; in particular, Figures 3b and 3d indicate that the interior distributions of Cl^- and Br^- become more favorable when the temperature rises to 340 K. Moreover, the surface propensity changes of Br^- also influence the spatial distribution of NH_4^+. At the lower temperature T = 280 K, the surface congregation of more Br^- anions leads to a subsurface accumulation of NH_4^+, while at the higher temperature T = 340 K, this subsurface peak in Figure 3c disappears and correspondingly the surface propensity of Br^- is also much weaker (see Figure 3d). However, as shown in Figures 3a and 3e, the spatial distributions of NH_4^+ in the $NH_4^+Cl^-$ and $NH_4^+I^-$ aqueous solutions are almost independent of the temperatures.

To further elucidate the thermodynamics mechanism of the surface propensity, the free energy profiles of NH_3, Br^-, and I^- across the interface are explored. In the MD simulation, the free energy profile is determined by the density profile of the solute in the water slab[35]

dx.doi.org/10.1021/jp312110w | J. Phys. Chem. C 2013, 117, 13011−13020

$$\Delta G(z) = -RT \ln \frac{\rho(z)}{\rho_b} \quad (1)$$

where R is the gas constant and ρ_b is the bulk density in the liquid phase. Since NH_3, Br^-, and I^- are significantly accumulated around the solution−air interface, their free energy profiles usually have the minimal values near the interface. Here, for the convenience of comparison, the density ρ_b in eq 1 is replaced with a normalization form $\rho_b(N_s/N_w)$ where N_s is the total number of solute molecules and N_w is the total number of water molecules. One can find in Figure 4 that

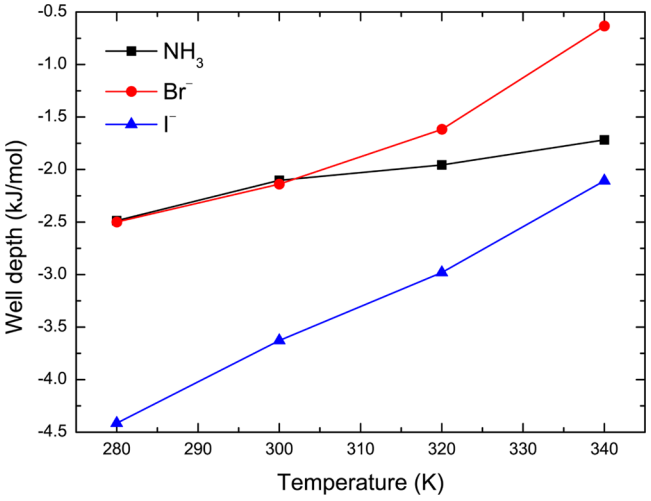

Figure 4. Minimal value in the free energy profile for NH_3 (square), Br^- (circle), and I^- (triangle) as a function of the temperature.

the minimal values monotonously decrease with the temperature enhancement. The positive variation slope of this value as a function of temperature indicates that the excess entropy for the NH_3, Br^-, and I^- moving from the bulk region to the interface region is negative; i.e., the entropic contribution disfavors the presence of these particles at the solution−air interface, which is consistent with the conclusion obtained by Netz and Horinek.[3]

3.2. Charge Distribution. The charge distribution around the solution−air interface is an important feature of electrolyte solution. It directly influences the interfacial electrostatic potential which not only plays an important role in a variety of fields ranging from atmospheric chemistry[47] to biophysics and biochemistry[48,49] but also is regarded as the indicator of molecular orientation at the interface. Meanwhile, the density profiles of NH_4^+ and the anions shown in Figures 2 and 3 indicate an electric double layer near the solution−air interface. This structure can be further evidenced in the charge distribution. The time-averaged charge distribution is calculated by counting the net charge near the Gibbs surface. The one-dimensional charge distribution of the $NH_4^+X^-$ solution is depicted in Figure 5 (the x-axis represents the distance from the Gibbs surface: $x < 0$ for the solution phase and $x > 0$ for the air phase), in which the profile is calculated as a ratio between the local and the global mole fractions of ion. For all of the simulated systems, the $NH_4^+X^-$ system shows the negative charge distribution near the Gibbs surface (-2 Å $< x <$ 2 Å), while the interior region ($x < -3$ Å) is positively charged. This is attributed to the higher surface propensity of X^- (Cl^-, Br^-, and I^-) and the higher interior propensity of NH_4^+. Under the

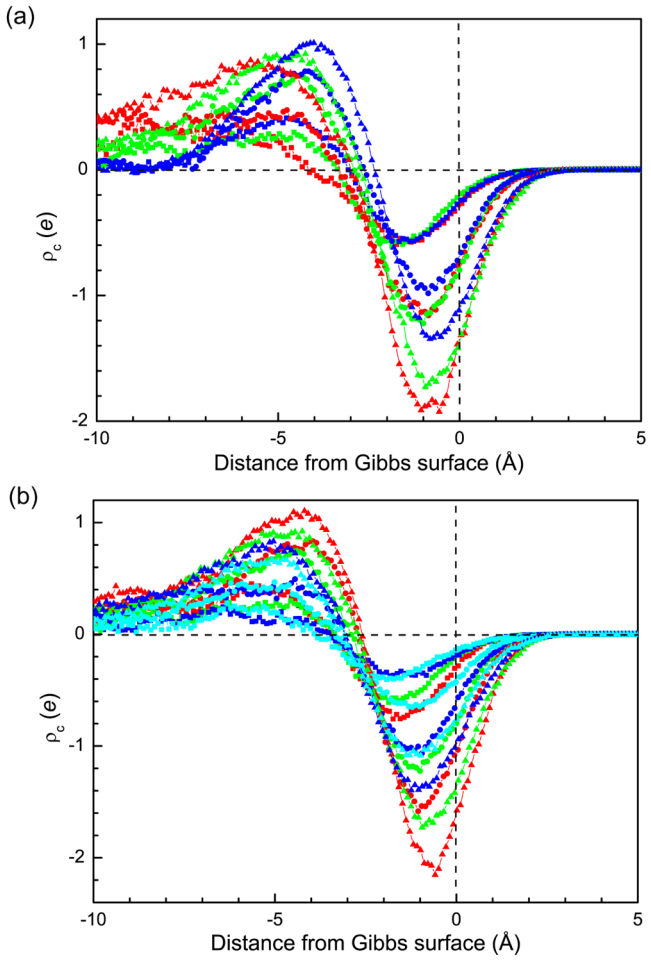

Figure 5. Concentration and temperature effects on the charge density (ρ_c) distribution. (a) The ρ_c distribution for $NH_4^+Cl^-$ (square), $NH_4^+Br^-$ (circle), and $NH_4^+I^-$ (triangle) with c = 0.55 M (red), 1.07 M (green), and 2.05 M (blue), respectively. (b) The ρ_c distribution for $NH_4^+Cl^-$ (square), $NH_4^+Br^-$ (circle), and $NH_4^+I^-$ (triangle) with T = 280 K (red), 300 K (green), 320 K (blue), and 340 K (cyan), respectively. The x-axis represents the distance from the Gibbs surface ($x < 0$ is the solution phase and $x > 0$ is the air phase).

same conditions, the sequence of absolute charge values near the Gibbs surface is $NH_4^+Cl^- < NH_4^+Br^- < NH_4^+I^-$, which is the same as the order of surface propensity of $Cl^- < Br^- < I^-$. The concentration dependency is shown in Figure 5a. Near the Gibbs surface, the negative charge values for $NH_4^+Cl^-$ are almost the same; however, the negative charges for $NH_4^+Br^-$ and $NH_4^+I^-$ solutions reduce dramatically when the c value rises to 2.05 M. This is in accord with the decreases of the surface densities of these two anions (see Figures 2d and 2f). In the region of -7 Å $< x < -3$ Å, the positive charge value increases remarkably with the increase of c, owing to more NH_4^+ cations underneath the surface (see Figures 2a, 2c, and 2e). On the other hand, as shown in Figure 5b, with the rise of temperature the charge value becomes smaller in the region of -7 Å $< x <$ 2 Å, due to the similar temperature effect on the spatial distributions (as discussed above and seen in Figure 3). All simulations for the $NH_4^+X^-$ solution−air interfaces indicate that an electric double layer with the negatively charged surface is formed. This local electric field near the interface can induce much more strongly the orientation of water molecules in the

dx.doi.org/10.1021/jp312110w | J. Phys. Chem. C 2013, 117, 13011−13020

solution−air interface than that for the pure water−air interface, which will be discussed in the next subsection.

3.3. Molecular Orientation at the Interface. To quantitatively describe the microstructures at the interfaces for both the solute ions and water molecules, we will analyze the molecular orientations at the interfaces, particularly focusing on the temperature effects. The definitions of the molecular orientations are shown as the inside panels of Figure 6: θ is the tilt angle between the molecular axis (c) and the surface normal (z); the twist angle, ψ is the rotational angle about the molecular axis. The Gibbs surface is defined as the xy plane (at $\rho/\rho_b = 0.5$, see Figures 1−3) in the laboratory frame and shown as a yellow plane. The θ-related order parameter is[50]

$$\langle S_1 \rangle = \frac{1}{2}\langle 3\cos^2\theta - 1 \rangle \quad (2)$$

and the ψ-related parameter is[50]

$$\langle S_2 \rangle = \frac{\langle \sin\theta \cos 2\psi \rangle}{\langle \sin\theta \rangle} \quad (3)$$

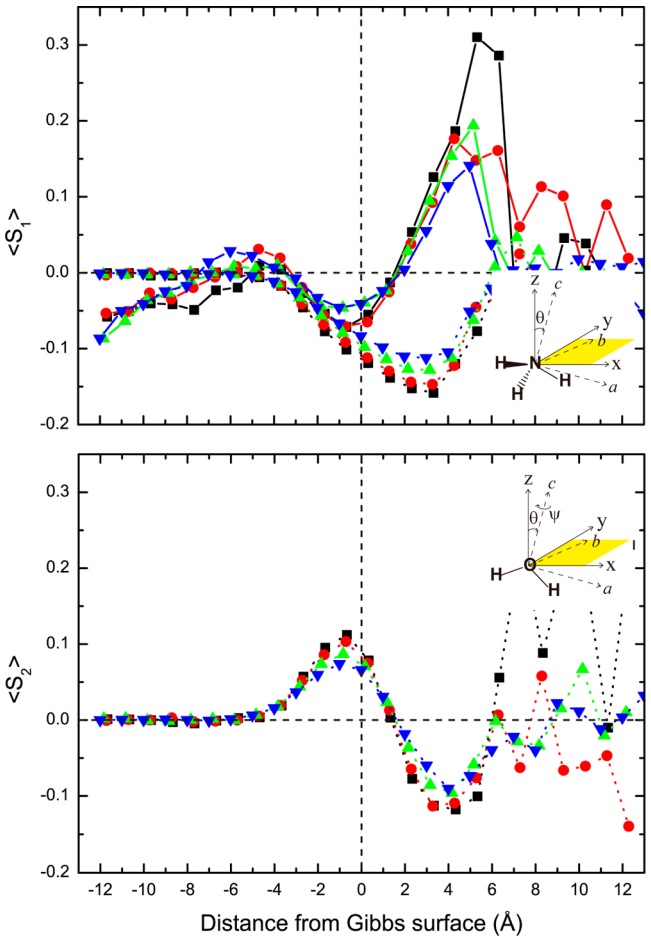

Figure 6. Tilt $\langle S_1 \rangle$ and twist $\langle S_2 \rangle$ order parameters for water (dotted lines) and NH_3 (solid lines) at the temperatures T = 280 K (square), 300 K (circle), 320 K (upward-pointing triangle), and 340 K (downward-pointing triangle). Inside panels illustrate the molecular orientations at the Gibbs surface (xy plane). The twist angle, ψ, parametrizes the rotation about the molecular c axis (the C_3 rotation axis of NH_3 and C_2 rotation axis in the H−O−H plane of water), and the tilt angle, θ, is defined as the angle between the z and c axes.

If we assume that the orientation preference for rotation about the C_3-symmetry molecular axis of NH_3 is very weak, $\langle S_1 \rangle$ will completely quantify the order. Due to the high symmetry of NH_4^+, the order parameters of NH_4^+ determined with eqs 2 and 3 can be ignored; however, $\langle S_2 \rangle$ should be considered for the water orientations. In general, $-0.5 < \langle S_1 \rangle < 1$ and $-1 < \langle S_2 \rangle < 1$. $\langle S_1 \rangle = 1$ indicates that all molecules are perfectly aligned with the C_2 (water) or C_3 (NH_3) axis parallel (or antiparallel) to the surface normal; the molecular axes are perpendicular to the surface normal when $\langle S_1 \rangle$ exactly equals −0.5.[50] The specific ψ value of 0° or 180° leads to $\langle S_2 \rangle = 1$, while $\langle S_2 \rangle = -1$ for ψ = 90° or 270°. The isotropic distribution should have zero values of these two order parameters.

For the NH_3 aqueous solution−air interface, the order parameters are plotted in Figure 6. The acute fluctuations of $\langle S_1 \rangle$ and $\langle S_2 \rangle$ in the region with a 5 Å or more distance away from the Gibbs surface (the vertical broken lines) are meaningless due to the extremely fewer molecules diffusing into air. In the region nearby the Gibbs surface (±5 Å), the orientations of water are specified; i.e., the negative $\langle S_1 \rangle$ (dotted lines) implies $54.7° < \langle \theta \rangle_{H_2O} < 125.2°$. In the region nearby the Gibbs surface (−5 to 1 Å), the positive $\langle S_2 \rangle$ corresponds to $0° < \langle \psi \rangle_{H_2O} < 45°$. When the water molecules are more than 1 Å away from the Gibbs surface, they rotate about the C_2 axis with the angles larger than 45°. Tow specific regions with the negative $\langle S_1 \rangle$ for NH_3 (solid lines) are also found, i.e., near the Gibbs surface (−3 to 1 Å) and in the inner region (−7 Å or more). However, in the outer region 2−5 Å away from the Gibbs surface, the NH_3 molecules prefer the alignment along their C_3 axes (parallel or antiparallel to the interface normal), while water molecules still tend to be perpendicular to the interface normal. Usually at the water−air interface, water molecules have the dangling OH bonds. Therefore, these NH_3 molecules are aligned via the intermolecular hydrogen bonding interaction with water molecules or between each other. Such a configuration of the NH_3−water complex at the interface is consistent with the observations of the SFG spectra;[31] i.e., the C_3 axis of NH_3 has the orientation angle of $25° \leq \theta \leq 38°$ with respect to the surface normal; the dipole moment of NH_3 points to the air phase; and the hydrogen bonds O−H···N are formed between NH_3 and water. When the temperature arises, both $\langle S_1 \rangle$ and $\langle S_2 \rangle$ values decrease due to the thermally stochastic motions of the interface molecules.

The order parameters of water molecules for $NH_4^+X^-$ (X^- = Cl^-, Br^-, I^-) are shown in Figure 7. The $\langle S_1 \rangle$ profiles of water molecules are similar to those in the NH_3 solution−air interface (see Figure 6). The orientation of water molecules is isotropic in the inner region (−5 Å or more), while in the neighborhood of the Gibbs surface (−5−5 Å) the C_2 axes of water molecules are slightly favored to be perpendicular to the interface normal. With the increase of temperature, the $\langle S_1 \rangle$ and $\langle S_2 \rangle$ values around the surface decrease. The tendency of $\langle S_2 \rangle$ shown in Figure 7 is also similar to that shown in Figure 6; however, some differences between them can be observed. For the $NH_4^+X^-$ solution−air systems, $\langle S_2 \rangle$ is negative in the region of −7 ∼ −4 Å, implying that the water molecule tends to twist with an angle value between 45° and 90°. The SFG study of 2 M $NH_4^+Cl^-$ solution indicated that the electric double layer led to a thicker interfacial region with the orientational polarization of water molecules than that for pure water.[34,37] Here the electric double layer is also predicted. To confirm this

dx.doi.org/10.1021/jp312110w | J. Phys. Chem. C 2013, 117, 13011−13020

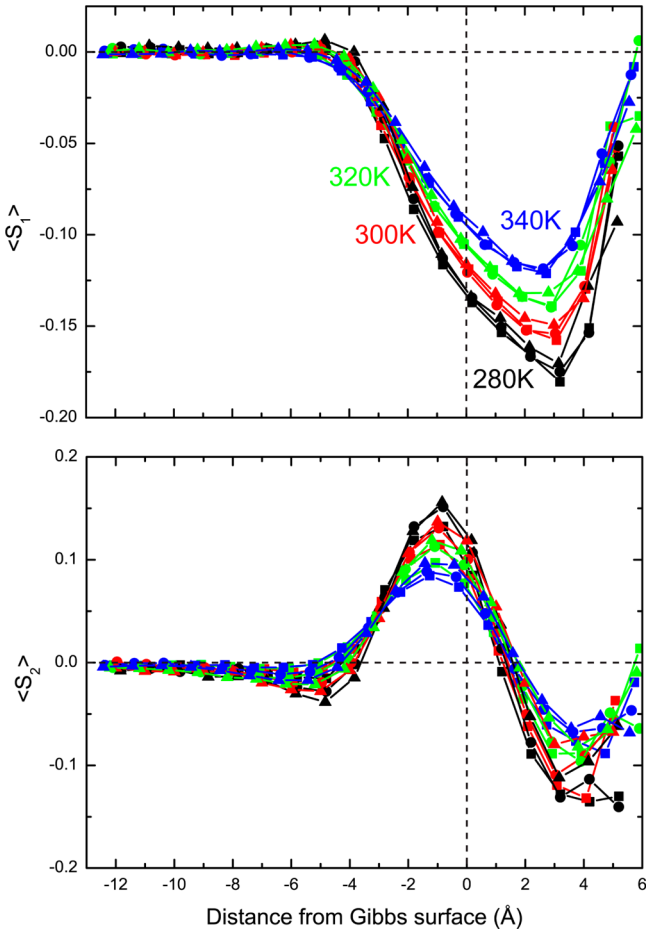

Figure 7. Tilt $\langle S_1 \rangle$ and twist $\langle S_2 \rangle$ order parameters for water at the different temperatures for the $NH_4^+X^-$ solution−air interfaces: X^- = Cl^- (square), Br^- (circle), and I^- (triangle).

phenomenon, the orientational polarization, i.e., $\langle \cos\theta \rangle$ as a function of the distance from the Gibbs surface, has been plotted in Figure 8. The $\langle \cos\theta \rangle$ value equals zero for the isotropic orientation of water dipoles, while its nonzero value

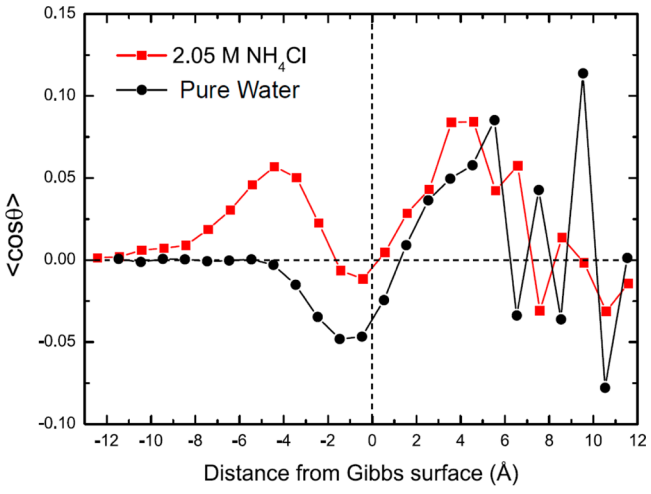

Figure 8. Orientational polarization parameter $\langle \cos\theta \rangle$ of 2.05 M $NH_4^+Cl^-$ (square) and pure water (circle) as functions of the distance from the Gibbs surface (x < 0 is the solution phase, and x > 0 is the air phase).

indicates a net orientation of water dipoles. The $\langle \cos\theta \rangle$ value for 2.05 M $NH_4^+Cl^-$ solution becomes nonzero and positive from the position of −10 Å, while its nonzero negative value begins with the position of −5 Å for pure water. One can find that the layer with the nonzero values of $\langle \cos\theta \rangle$ is much thicker in the 2.05 M $NH_4^+Cl^-$ solution. This is attributed to a formation of the electric double layer near the Gibbs surface.[34,37]

3.4. Surface Tension. Besides the temperature effect on the surface microstructures, we also investigate the temperature influences on surface tension. The microscopic theory of surface tension (γ) is based on the Gibbs adsorption equation.[51,52] In the case of MD simulations for the slab geometry[53]

$$\gamma = \frac{1}{2} L_z \left\langle P_{zz} - \frac{1}{2}(P_{xx} + P_{yy}) \right\rangle \quad (4)$$

where L_z is the length of the box in the z direction; the P_{ii} are the diagonal components of the pressure tensor; and the prefactor 1/2 accounts for the presence of two interfaces in the slab. The calculated results together with the statistical uncertainties[54] are depicted in Figure 9. In Figure 9(a), the relative values of surface tension for NH_3 solution with respect to that for the pure water are close to each other for c = 0.55 and 1.07 M but go down significantly when the c value rises from 1.07 to 2.05 M. As for the other solutions, the variation tendencies of surface tension with the increase of c are distinctly different. Within statistical uncertainty, the surface tension of $NH_4^+Cl^-$ becomes larger, while that of $NH_4^+I^-$ decreases with the rise of c. It is noted that the surface tensions of both NaCl and NaI solutions were also found to be enhanced with the rise of c.[55] This discrepancy arises from the facts that the relative Na^+ distribution was reduced with the increase of c for NaI (see Figure 6b in ref 55), but here the surface propensity of NH_4^+ in the $NH_4^+I^-$ solution−air interface is significantly enhanced (see Figure 2e). The surface tension variances for $NH_4^+Cl^-$ and $NH_4^+Br^-$ are ambiguous due to the large uncertainties.

The temperature-dependent surface tensions (c = 1.07 M) are depicted in Figure 9(b). The calculated results are shifted and calibrated with a reference to the experimental datum of the water−air system[56] at 280 K. In the previous study of the sodium-halide salts, the order of γ values was NaI < NaBr < NaCl < NaF (at room temperature and c = 1.2 M).[2] In the present case, a similar order $NH_4^+I^-$ < $NH_4^+Br^-$ < $NH_4^+Cl^-$ is predicted at T = 300 K, and this sequence is held at the lower and higher temperatures. The calculated γ values for both the solutions and pure water decrease with the rise of temperature, which is in line with our common sense. One can find that in this temperature range the γ values for $NH_4^+Br^-$ and $NH_4^+Cl^-$ are higher or not less than that of pure water, while the relative γ values for $NH_4^+I^-$ and NH_3 are varied a little with temperature. Such observations have never been reported prior to this work, which deserves further investigations on the temperature effect.

4. CONCLUSION

In the present study, the classical MD simulations of the interfaces of NH_3 and $NH_4^+X^-$ (X^- = Cl^-, Br^-, and I^-) aqueous solution−air are performed with the polarizable force fields AMOEBA 09.[38−40] The spatial distributions of ions, the charge distribution, the molecular orientations, and the surface

dx.doi.org/10.1021/jp312110w | J. Phys. Chem. C 2013, 117, 13011−13020

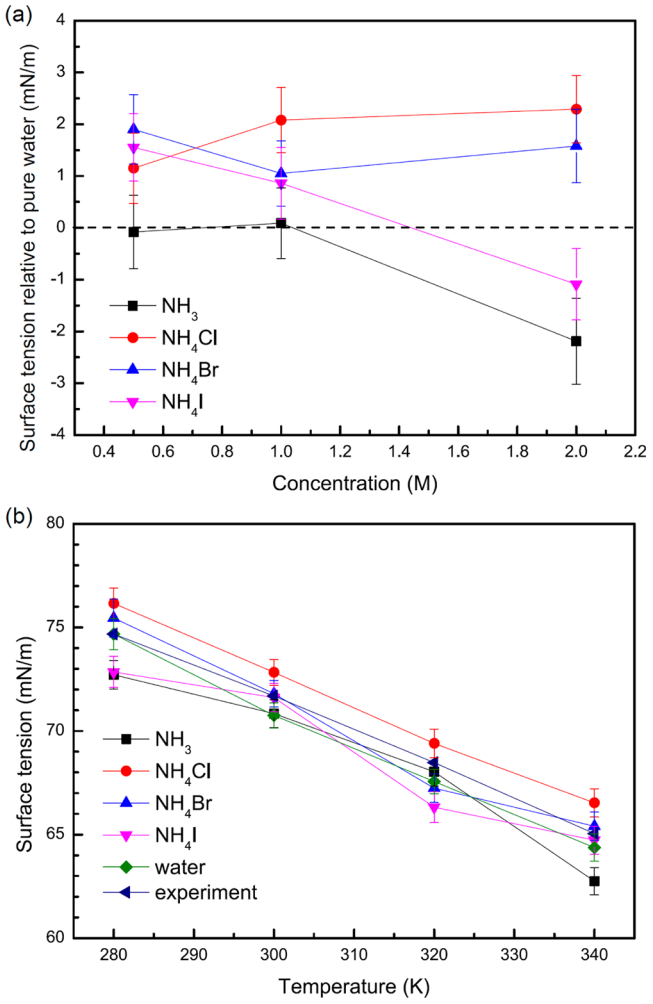

Figure 9. Concentration and temperature effects on the surface tensions. (a) The concentration dependences for NH_3 (square) and $NH_4^+Cl^-$ (circle), $NH_4^+Br^-$ (upward-pointing triangle), and $NH_4^+I^-$ (downward-pointing triangle), with respect to the surface tension for pure water (broken line). (b) The temperature dependences for NH_3 (square), $NH_4^+Cl^-$ (circle), $NH_4^+Br^-$ (upward-pointing triangle), $NH_4^+I^-$ (downward-pointing triangle), and water (rhombus), and the experimental data (ref 56) of the water–air interface (left-pointing triangle). The calculated results are shifted with a reference of the experimental datum of the water–air interface at 280 K.

tensions are analyzed in terms of the different concentrations and temperatures. Our remarks are summarized here:

(a) The NH_3, Br^-, and I^- species exhibit more significant surface propensities than that of Cl^-, while the NH_4^+ prefers the interior region. When the concentration increases, the surface propensities of NH_3, Br^-, and I^- become weaker, but the surface propensity of the Cl^- anion shows an enhancement for the higher concentration c = 2.05 M. The surface propensities of NH_3, Cl^-, Br^-, and I^- clearly decline when the temperature rises, indicating that the entropic contribution disfavors the presence of these species at the solution–air interface. Nevertheless, the temperature effect on the spatial distribution of NH_4^+ is weak, in particular, for the solution–air interfaces of $NH_4^+X^-$ (X^- = Cl^-, I^-). The distinctly different surface propensities of NH_4^+ and the halogen anions lead to the formation of an electric double layer near the interface. The charge is negative near the Gibbs surface of $NH_4^+X^-$ solution–air interfaces, while the charge is positive in the interior region. The charge distribution of this electric double layer strongly influences the orientations of water molecules. Under the same conditions, the order of absolute charge values for these three electrolyte solutions near the Gibbs surface is $NH_4^+Cl^- < NH_4^+Br^- < NH_4^+I^-$, which is consistent with the order of surface propensity of $Cl^- < Br^- < I^-$.

(b) When the temperature is enhanced, the molecular orientations for NH_3 and water at the interface are less anisotropic due to the thermally stochastic motions of the molecules. The difference of the orientational polarization of water molecules between the pure water liquid and the 2.05 M $NH_4^+Cl^-$ solution is attributed to the specific electric double layer formed near the solution–air interface.

(c) The surface tension variation with the solute concentration is highly complex, but it is mainly attributed to the different surface propensities of ions. On the other hand, the surface tensions reduce with the increase of temperature. The temperature effects on the molecular orientations at the interface and the surface tensions are explored here for the first time and deserve further investigations in the future.

AUTHOR INFORMATION

Corresponding Author

*E-mail: sxtian@ustc.edu.cn.

Notes

The authors declare no competing financial interest.

ACKNOWLEDGMENTS

This work is supported by CAS (Grant No. KJCX2-EW-W09) and the Fundamental Research Funds for the Central Universities (Grant No.WK2340000012). The numerical calculations have been done on the supercomputing system in the Supercomputing Center of University of Science and Technology of China.

REFERENCES

(1) *Draft 2009 update aquatic life ambient water quality criteria for ammonia- freshwater*; U.S. Environmental Protection Agency: Washington, DC, Dec. 2009.

(2) Jungwirth, P.; Tobias, D. J. Specific Ion Effects at the Air/Water Interface. *Chem. Rev.* **2006**, *106*, 1259–1281.

(3) Netz, R. R.; Horinek, D. Progress in Modeling of Ion Effects at the Vapor/Water Interface. *Annu. Rev. Phys. Chem.* **2012**, *63*, 401–418.

(4) Wilson, M. A.; Pohorille, A.; Pratt, L. R. Molecular Dynamics of the Water Liquid–Vapor Interface. *J. Phys. Chem.* **1987**, *91*, 4873–4878.

(5) Wilson, M. A.; Pohorille, A. Interaction of Monovalent Ions with the Water Liquid–Vapor Interface: A Molecular Dynamics Study. *J. Chem. Phys.* **1991**, *95*, 6005–6013.

(6) Benjamin, I. Theoretical Study of Ion Solvation at the Water Liquid-Vapor Interface. *J. Chem. Phys.* **1991**, *95*, 3698–3709.

(7) Vrbka, L.; Mucha, M.; Minofar, B.; Jungwirth, P.; Brown, E. C.; Tobias, D. J. Propensity of Soft Ions for the Air/Water Interface. *Curr. Opin. Colloid Interface Sci.* **2004**, *9*, 67–73.

(8) Herce, D. H.; Perera, L.; Darden, T. A.; Sagui, C. Surface Solvation for an Ion in a Water Cluster. *J. Chem. Phys.* **2005**, *122*, 024513.

(9) Hagberg, D.; Brdarski, S.; Karlstrom, G. On the Solvation of Ions in Small Water Droplets. *J. Phys. Chem. B* **2005**, *109*, 4111–4117.

(10) Dang, L. X.; Chang, T. M. Molecular Mechanism of Ion Binding to the Liquid/Vapor Interface of Water. *J. Phys. Chem. B* **2002**, *106*, 235–238.

(11) Dang, L. X. Computational Study of Ion Binding to the Liquid Interface of Water. *J. Phys. Chem. B* **2002**, *106*, 10388–10394.

(12) Stuart, S. J.; Berne, B. J. Surface Curvature Effects in Aqueous Ionic Solvation of the Chloride Ion. *J. Phys. Chem. A* **1999**, *103*, 10300−10307.
(13) Jungwirth, P.; Tobias, D. J. Surface Effects on Aqueous Ionic Solvation: A Molecular Dynamics Simulation Study of NaCl at the Air/Water Interface from Infinite Dilution to Saturation. *J. Phys. Chem. B* **2000**, *104*, 7702−7706.
(14) Jungwirth, P.; Tobias, D. J. Molecular Structure of Salt Solutions: A New View of the Interface with Implications for Heterogeneous Atmospheric Chemistry. *J. Phys. Chem. B* **2001**, *105*, 10468−10472.
(15) Petersen, P. B.; Saykally, R. J.; Mucha, M.; Jungwirth, P. Enhanced Concentration of Polarizable Anions at the Liquid Water Surface: SHG Spectroscopy and MD Simulations of Sodium Thiocyanide. *J. Phys. Chem. B* **2005**, *109*, 10915−10921.
(16) Tuma, L.; Jenicek, D.; Jungwirth, P. Propensity of Heavier Halides for the Water/Vapor Interface Revisited Using the Amoeba Force Field. *Chem. Phys. Lett.* **2005**, *411*, 70−74.
(17) Randalls, J. E. B. Structure at the Free Surface of Water and Aqueous Electrolyte Solutions. *Phys. Chem. Liq.* **1977**, *7*, 107−179.
(18) Onsager, L.; Samaras, N. N. T. The Surface Tension of Debye-Hückel Electrolytes. *J. Chem. Phys.* **1934**, *2*, 528−536.
(19) Salvador, P.; Curtis, J. E.; Tobias, D. J.; Jungwirth, P. Polarizability of the Nitrate Anion and Its Solvation at the Air/Water Interface. *Phys. Chem. Chem. Phys.* **2003**, *5*, 3752−3757.
(20) Yang, X.; Kiran, B.; Wang, X. B.; Wang, L. S.; Mucha, M.; Jungwirth, P. Solvation of the Azide Anion (N_3^-) in Water Clusters and Aqueous Interfaces: A Combined Investigation by Photoelectron Spectroscopy, Density Functional Calculations, and Molecular Dynamics Simulations. *J. Phys. Chem. A* **2004**, *108*, 7820−7826.
(21) Jungwirth, P.; Curtis, J. E.; Tobias, D. J. Polarizability and Aqueous Solvation of the Sulfate Dianion. *Chem. Phys. Lett.* **2003**, *367*, 704−710.
(22) Dang, L. X. Solvation of the Hydronium Ion at the Water Liquid/Vapor Interface. *J. Chem. Phys.* **2003**, *119*, 6351−6353.
(23) Petersen, M. K.; Iyengar, S. S.; Day, T. J. F.; Voth, G. A. The Hydrated Proton at the Water Liquid/Vapor Interface. *J. Phys. Chem. B* **2004**, *108*, 14804−14806.
(24) Mucha, M.; Frigato, T.; Levering, L. M.; Allen, H. C.; Tobias, D. J.; Dang, L. X.; Jungwirth, P. Unified Molecular Picture of the Surfaces of Aqueous Acid, Base, and Salt Solutions. *J. Phys. Chem. B* **2005**, *109*, 7617−7623.
(25) Yang, L.; Fan, Y.; Gao, Y. Q. Differences of Cations and Anions: Their Hydration, Surface Adsorption, and Impact on Water Dynamics. *J. Phys. Chem. B* **2011**, *115*, 12456−12465.
(26) Ishiyama, T.; Morita, A. Molecular Dynamics Simulation of Sum Frequency Generation Spectra of Aqueous Sulfuric Acid Solution. *J. Phys. Chem. C* **2011**, *115*, 13704−13716.
(27) Ishiyama, T.; Morita, A.; Miyamae, T. Surface Structure of Sulfuric Acid Solution Relevant to Sulfate Aerosol: Molecular Dynamics Simulation Combined with Sum Frequency Generation Measurement. *Phys. Chem. Chem. Phys.* **2011**, *13*, 20965−20973.
(28) Annapureddy, H. V. R.; Dang, L. X. Molecular Mechanism of the Adsorption Process of an Iodide Anion into Liquid−Vapor Interfaces of Water−Methanol Mixtures. *J. Chem. Phys.* **2012**, *137*, 214705.
(29) Vazdar, M.; Pluhařová, E.; Mason, P. E.; Vácha, R.; Jungwirth, P. Ions at Hydrophobic Aqueous Interfaces: Molecular Dynamics with Effective Polarization. *J. Phys. Chem. Lett.* **2012**, *3*, 2087−2091.
(30) Simonelli, D.; Baldelli, S.; Shultz, M. J. Ammonia−Water Complexes on the Surface of Aqueous Solutions Observed with Sum Frequency Generation. *Chem. Phys. Lett.* **1998**, *298*, 400−404.
(31) Simonelli, D.; Shultz, M. J. Sum Frequency Generation Orientation Analysis of Molecular Ammonia on the Surface of Concentrated Solutions. *J. Chem. Phys.* **2000**, *112*, 6804−6816.
(32) Dang, L. X.; Garrett, B. C. Molecular Mechanism of Water and Ammonia Uptake by the Liquid/Vapor Interface of Water. *Chem. Phys. Lett.* **2004**, *385*, 309−313.
(33) Paul, S.; Chandra, A. Liquid−Vapor Interfacial Properties of Water−Ammonia Mixtures: Dependence on Ammonia Concentration. *J. Chem. Phys.* **2005**, *123*, 174712.
(34) Gopalakrishnan, S.; Jungwirth, P.; Tobias, D. J.; Allen, C. Air−Liquid Interfaces of Aqueous Solutions Containing Ammonium and Sulfate: Spectroscopic and Molecular Dynamics Studies. *J. Phys. Chem. B* **2005**, *109*, 8861−8872.
(35) Carignano, M. A.; Jacob, M. M.; Avila, E. E. On the Uptake of Ammonia by the Water/Vapor Interface. *J. Phys. Chem. A* **2008**, *112*, 3676−3679.
(36) Chakraborty, D.; Chandra, A. Hydrogen Bonded Structure and Dynamics of Liquid−Vapor Interface of Water−Ammonia Mixture: An ab initio Molecular Dynamics Study. *J. Chem. Phys.* **2011**, *135*, 114510.
(37) Tian, C.; Byrnes, S. J.; Han, H.-L.; Shen, Y. R. Surface Propensities of Atmospherically Relevant Ions in Salt Solutions Revealed by Phase-Sensitive Sum Frequency Vibrational Spectroscopy. *J. Phys. Chem. Lett.* **2011**, *2*, 1946−1949.
(38) Ren, P.; Ponder, J. W. Consistent Treatment of Inter- and Intramolecular Polarization in Molecular Mechanics Calculations. *J. Comput. Chem.* **2002**, *23*, 1497−1506.
(39) Ren, P.; Ponder, J. W. Polarizable Atomic Multipole Water Model for Molecular Mechanics Simulation. *J. Phys. Chem. B* **2003**, *107*, 5933−5947.
(40) Ponder, J. W.; Case, D. A. Force Fields for Protein Simulations. *Adv. Protein Chem.* **2003**, *66*, 27−85.
(41) Grossfield, A.; Ren, P.; Ponder, J. W. Ion Solvation Thermodynamics from Simulation with a Polarizable Force Field. *J. Am. Chem. Soc.* **2003**, *125*, 15671−15682.
(42) Using TINKER - Software Tools for Molecular Design package, http://dasher.wustl.edu/tinker/ (accessed June, 2011).
(43) Swope, W. C.; Andersen, H. C.; Berens, P. H.; Wilson, K. R. A Computer Simulation Method for the Calculation of Equilibrium Constants for the Formation of Physical Clusters of Molecules: Application to Small Water Clusters. *J. Chem. Phys.* **1982**, *76*, 637−649.
(44) Berendsen, H. J. C.; Postma, J. P. M.; DiNola, A.; Haak, J. R. Molecular Dynamics with Coupling to an External Bath. *J. Chem. Phys.* **1984**, *81*, 3684−3690.
(45) Essman, U.; Perela, L.; Berkowitz, M. L.; Darden, T.; Lee, H.; Pedersen, L. G. A Smooth Particle Mesh Ewald Method. *J. Chem. Phys.* **1995**, *103*, 8577−8593.
(46) Andersen, H. C. Rattle: A "Velocity" Version of the Shake Algorithm for Molecular Dynamics Calculations. *J. Comput. Phys.* **1983**, *52*, 24−34.
(47) Hu, J. H.; Shi, Q.; Davidovits, P.; Worsnop, D. R.; Zahniser, M. S.; Kolb, C. E. Reactive Uptake of Cl_2(g) and Br_2(g) by Aqueous Surfaces as a Function of Br^- and I^- Ion Concentration: The Effect of Chemical Reaction at the Interface. *J. Phys. Chem.* **1995**, *99*, 8768−8776.
(48) Zhang, Y. J.; Cremer, P. S. Interaction between Macromolecules and Ions: The Hofmeister Series. *Curr. Opin. Chem. Biol.* **2006**, *10*, 658−663.
(49) Ostroumova, O. S.; Malev, V. V.; Bessonov, A. N.; Takemoto, J. Y.; Schagina, L. V. Altering the Activity of Syringomycin E via the Membrane Dipole Potential. *Langmuir* **2008**, *24*, 2987−2991.
(50) Buffeteau, T.; Lagugné Labarthet, F.; Sourisseau, C.; Kostromine, S.; Bieringer, T. Biaxial Orientation Induced in a Photoaddressable Azopolymer Thin Film As Evidenced by Polarized UV-Visible, Infrared, and Raman Spectra. *Macromolecules* **2004**, *37*, 2880−2889.
(51) Fawcett, W. R. *Liquids, Solutions, and Interfaces*; Oxford Press: Oxford, 2004.
(52) Petersen, P. B.; Saykally, R. J. Adsorption of Ions to the Surface of Dilute Electrolyte Solutions: The Jones-Ray Effect Revisited. *J. Am. Chem. Soc.* **2005**, *127*, 15446−15452.
(53) Rowlinson, J. S.; Widom, B. *Molecular Theory of Capilarity*; Oxford Science Publications: Oxford, 1982.

(54) Allen, M. P.; Tildesley, D. J. *Computer simulation of liquid*; Clarendon Press: Oxford, 1987; pp 191−198.
(55) Ishiyama, T.; Morita, A. Molecular Dynamics Study of Gas-Liquid Aqueous Sodium Halide Interfaces. I. Flexible and Polarizable Molecular Modeling and Interfacial Properties. *J. Phys. Chem. C* **2007**, *111*, 721−737.
(56) Vargaftik, N. B.; Volkov, B. N.; Voljak, L. D. International Tables of the Surface Tension of Water. *J. Phys. Chem. Ref. Data* **1983**, *12*, 817−820.